

Sterile neutrinos as subdominant warm dark matter

A. Palazzo^{1,2}, D. Cumberbatch¹, A. Slosar¹, and J. Silk¹

¹ *Astrophysics, Denys Wilkinson Building,
Keble Road, OX1 3RH,
Oxford, United Kingdom*

² *Sezione INFN di Bari,
Via Amendola 173, 70126, Bari, Italy*

Abstract

In light of recent findings which seem to disfavor a scenario with (warm) dark matter entirely constituted of sterile neutrinos produced via the Dodelson-Widrow (DW) mechanism, we investigate the constraints attainable for this mechanism by relaxing the usual hypothesis that the relic neutrino abundance must necessarily account for all of the dark matter. We first study how to reinterpret the limits attainable from X-ray non-detection and Lyman- α forest measurements in the case that sterile neutrinos constitute only a fraction f_s of the total amount of dark matter. Then, assuming that sterile neutrinos are generated in the early universe solely through the DW mechanism, we show how the X-ray and Lyman- α results jointly constrain the mass-mixing parameters governing their production. Furthermore, we show how the same data allow us to set a robust upper limit $f_s \lesssim 0.7$ at the 2σ level, rejecting the case of dominant dark matter ($f_s = 1$) at the $\sim 3\sigma$ level.

PACS numbers: 95.35.+d,14.60.Pq,14.60.St

I. INTRODUCTION

Recent astrophysical observations, such as the indications of central cores in low-mass galaxies [1, 2, 3, 4, 5, 6, 7, 8, 9], and the low number of satellites observed in Milky Way-sized galaxies [10, 11, 12], indicate two possible shortcomings of the $[\Lambda]$ CDM paradigm (see [13, 14]) and have boosted the interest in a warm dark matter (WDM) scenario which may alleviate these possible small scale problems [15, 16]. Electroweak singlet right handed (“sterile”) neutrinos ν_s with mass in the keV range appear to be appealing candidates since they naturally arise in many extensions [17, 18, 19, 20, 21, 22] of the Standard Model and they could be produced in the early universe through the Dodelson-Widrow (DW) mechanism [23] involving (non-resonant) oscillations with the active species.

Direct constraints on mass and mixing angle of the sterile neutrino¹ can be obtained by exploiting X-ray observations [26, 27, 28, 29]. Indeed, sterile neutrinos possess a radiative decay channel [30, 31], which gives rise to photons potentially detectable in astrophysical X-ray and γ -ray sources. Limits of such kind have been derived exploiting diffuse cosmic X-ray background [27, 32], Milky Way “blank sky” observations [33, 34, 35, 36], X-ray spectra of nearby galaxies [35, 37] or clusters of galaxies [38, 39, 40], and gamma-ray line emission searches in the galactic center region [41]. *Indirect* constraints on the neutrino mass can be achieved by the observations of cosmological structure formation on very small scales, where WDM typically suppresses the clustering process. In this context, Lyman- α forest measurements (henceforth Ly- α) constitute the most suitable probe [42], being sensitive tracers of the primordial density fluctuations on the smallest scales.

Assuming that sterile neutrinos are produced *solely* through the DW mechanism and requiring that they must account for *all* the dark matter density $\Omega_s = \Omega_{\text{dm}}$, the recent X-ray analyses [32, 33, 34, 35, 36, 37, 38, 39, 40] determine upper limits on their mass which lie in the range (3-8 keV). On the other hand, under the same hypotheses, the latest Ly- α analyses [43, 44] of the high redshift flux power spectra, measured by the SDSS survey [45], furnish lower bounds in the range (10-13 keV), in clear tension with the X-ray upper limits.²

While these results imply that sterile neutrinos cannot account for the *entire* amount of dark matter in the universe,³ the possibility exists that the DW mechanism could have produced only a fraction $f_s = \Omega_s/\Omega_{\text{dm}}$ of its total content. This does not prevent sterile neutrinos from playing an important role in other contexts, such as pulsar kicks [52, 53, 54, 55, 56], supernova explosions [57, 58], and reionization of the universe [59, 60, 61, 62, 63, 64, 65]. Indeed, it has been already recognized [49] that a sterile neutrino explanation of the pulsar kicks can be reconciled with the existing X-ray constraints assuming the (lowest possible) relic abundance provided by the DW production mechanism. Furthermore, the suppression of small scale structures induced by WDM, while reducing problems at low redshifts, delays the onset of reionization [59, 60], possibly to an extent difficult to reconcile with the WMAP3 findings [66]. Whether the X-rays emitted by sterile neutrinos can effectively diminish this inconsistency is still an open question [62, 64, 65], and a subdominant ($f_s < 1$)

¹ Notice that the LSND [24] and MiniBooNE [25] experiments are not sensitive to the extremely small mixing angles involved in the DW mechanism.

² Similar lower bounds ($\gtrsim 10$ keV) have been determined by QSO gravitational lensing observations [46].

³ This conclusion can be evaded invoking alternative production mechanisms (not considered in this work), such as resonant oscillations [47], generation operative during [48] or prior to [49] oscillations or low reheating temperatures [50, 51].

relic abundance would probably reduce the tension also in this context.

Therefore, it seems interesting to investigate in a systematic way the constraints attainable on the mass-mixing parameters which regulate the DW production mechanism relaxing the usual assumption of “dominant” dark matter ($\Omega_s = \Omega_{\text{dm}}$). With this purpose in mind, we first address the issue of reinterpreting the X-ray and Ly- α constraints in the presence of a ν_s subdominant relic abundance ($\Omega_s < \Omega_{\text{dm}}$) which is fixed *a priori*, i.e. independently of the oscillation parameters. Then, we treat the general case in which the relic abundance depends on mass-mixing parameters as predicted by the DW mechanism. We determine the range of such parameters that is compatible with the restrictions imposed by the joint analysis of X-ray and Ly- α measurements. In addition, we show how these results indirectly compel the relic abundance to be smaller than $f_s \lesssim 70\%$ (at the 2σ level), even when the large (hadronic) uncertainties affecting the theoretical calculations are taken into account.

The paper is structured as follows. In Sec. II, we present our constraints obtained from the diffuse X-ray background, briefly discussing their behavior for values of $f_s < 1$. In Sec. III, we introduce a recipe to derive lower bounds on the sterile neutrino mass for values $f_s < 1$, appropriately rescaling the Ly- α limits already existing for the usual case $f_s = 1$. In Sec. IV, we show how the tension existing between X-ray and Ly- α constraints is reduced when the sterile neutrinos are subdominant. In Sec. V, we discuss the restrictions imposed on the mass-mixing parameters by the joint analysis of X-ray and Ly- α data, also determining the maximum value of the relic abundance allowed by current data. Finally, we present our conclusions in Sec. VI.

II. CONSTRAINTS FROM DIFFUSE X-RAY DATA

Sterile neutrinos possess a (subdominant) radiative decay channel $\nu_s \rightarrow \gamma\nu_a$ into an active neutrino ν_a and a photon γ with energy equal to a half of the sterile neutrino mass $E = m_s/2$. For Majorana neutrinos⁴ the radiative decay width can be expressed as⁵

$$\Gamma_\gamma = \frac{9\alpha G_F^2}{1024\pi^4} m_s^5 \sin^2 2\theta \simeq 1.38 \times 10^{-22} \sin^2 2\theta \left(\frac{m_s}{\text{keV}} \right)^5 \text{ s}^{-1}, \quad (1)$$

where G_F is the Fermi constant, α is the fine-structure constant and θ is the mixing angle in vacuum between the sterile neutrino and the active species which, for the very small values considered in this work, is related to the effective mixing angles θ_α ’s with each of the standard (active) neutrinos as,

$$\sin^2 \theta \simeq \theta^2 = \sum_{\alpha=e,\mu,\tau} \theta_\alpha^2. \quad (2)$$

In order to derive constraints from the diffuse X-ray background we use the data provided by the HEAO-1 detector [67, 68] since this experiment covers a large energy band, allowing us to put constraints up to large values of the mass (~ 50 keV). This becomes relevant when the hypothesis that sterile neutrinos are dominant is relaxed. Furthermore, these measurements have been shown to furnish stringent and robust constraints [32], which are comparable with those obtained from nearby galaxies [35, 37] or clusters of galaxies [38, 39, 40].

⁴ For a Dirac sterile neutrino the decay width is a half [31].

⁵ Throughout the paper we use natural units with $\hbar = c = k_B = 1$.

The signal expected in the HEAO-1 detector due to the decay of the putative dark matter candidate originates in part from the extra galactic (EG) neutrinos, and in part from neutrinos clustered in the Milky Way (MW) halo. The EG contribution can be evaluated assuming a uniform distribution of neutrinos in the visible universe up to very small redshifts. Defining F_E as the present energy flux of photons produced by neutrino decays, the differential energy flux (energy flux per unit energy and solid angle) can be expressed as [69]

$$\varphi_E^{\text{EG}} \equiv \frac{d^2 F_E^{\text{EG}}}{d\Omega dE} = f_s \frac{\Gamma_\gamma}{4\pi m_s} \frac{\Omega_{\text{dm}} \rho_c}{H(m_s/2E - 1)}, \quad (3)$$

where ρ_c is the present critical density, $\Omega_{\text{dm}} \simeq 0.20$ is its fraction in form of dark matter [66], and $H(z)$ is the Hubble function which, assuming a flat Λ -matter dominated universe, is related to the present expansion rate⁶ H_0 as

$$H(z) \simeq H_0 \sqrt{\Omega_\Lambda + \Omega_m(1+z)^3}, \quad (4)$$

where $\Omega_m \simeq 0.24$ and $\Omega_\Lambda \simeq 0.76$ are the present fractions of the critical density [66] in form of (total) matter and dark energy respectively.⁷

The monochromatic energy flux produced by the sterile neutrinos clustered in our galactic halo can be formally expressed as

$$\varphi_E^{\text{MW}} \equiv \frac{d^2 F_E^{\text{MW}}}{d\Omega dE} = f_s \frac{\Gamma_\gamma m_s}{8\pi 2E} S_{\text{dm}} \delta\left(E - \frac{m_s}{2}\right), \quad (5)$$

which depends on the direction through the mass column density S_{dm} of dark matter along the line of sight (l.o.s.),

$$S_{\text{dm}} = \int_{\text{l.o.s.}} \rho_{\text{dm}}(x) dx. \quad (6)$$

It is useful to compare the relative magnitude of the EG and MW contributions through the (directionally-dependent) ratio of their fluxes integrated over energy. From Eqs. (3-5) one gets

$$R_{\text{l.o.s.}} \equiv \frac{\int \varphi_E^{\text{MW}} dE}{\int \varphi_E^{\text{EG}} dE} \simeq 0.5 \left(\frac{S_{\text{dm}}}{10^{-2} \text{g cm}^{-2}} \right), \quad (7)$$

which, for typical mass column densities S_{dm} , turns out to be of order unity. In particular, adopting the recent evaluation of the galactic halo mass determined in [70] for a Navarro-Frenk-White profile, we find values of R in the 2σ range (0.5-3.0), in the direction of the galactic anti-center (corresponding to the lowest column density). In consideration of the all-sky coverage of the HEAO-1 detector [67, 68], we adopt the simple and conservative choice $R = 1$, thus assuming a MW contribution independent of direction. The effect of a more realistic treatment (requiring precise knowledge of the sky coverage of the detector during its time of operation) would only render our limits more stringent.

In order to find constraints on the mass-mixing parameters, we have performed a spectral analysis of the HEAO-1 data following the procedure described in [32], adding the EG and

⁶ $H_0 \simeq 100 h \text{ km s}^{-1} \text{ Mpc}^{-1}$ with $h = 0.73$ [66].

⁷ We have checked that the uncertainties on the cosmological parameters have a negligible impact on our results.

MW contributions to the continuous X-ray spectrum parameterized by the empirical formula provided in [68]. In Fig. 1 we show the region excluded at the 3σ level (above the curves) obtained in the case $f_s = 1$. For completeness, we show separately the constraints that we obtain including *only* the EG contribution (dotted line), and *only* the MW contribution (dashed line), together with the constraints obtained properly taking both contributions into account (solid line). Even if the total MW and EG fluxes have the same order of magnitude (exactly identical in our case), the MW contribution has a sensibly larger impact in determining the constraints. This different sensitivity is due to the different form of the energy spectrum produced in the two cases. Indeed, while the MW signal is just a line broadened into a (large) gaussian (centered around $E = m_s/2$) by the (poor) energy resolution ($\Delta E/E \simeq 25\%$) of the detector [68], the EG spectrum is intrinsically broadened towards low energies as a result of the integration over redshift and is further enlarged by the effect of the resolution of the detector. Both constraints obtained with or without the inclusion of the MW contribution are in good agreement with the analogous ones found respectively in [32] and [29]. Our bounds appear only slightly weaker when the MW contribution is also included, presumably due to the different choice adopted for the mass of the galactic halo.

As is evident from Eqs. (1-5), the differential flux produced by the decay of sterile neutrinos depends on the product $f_s \sin^2 2\theta$. Hence, for a fixed neutrino mass, the upper limit on the mixing angle must weaken for decreasing values of f_s , rescaling exactly as the inverse of the fraction f_s . This means that if one fixes *a priori* the fraction $f_s < 1$ (i.e. independently of the mass-mixing parameters), the excluded region in the plane $[m_s, \sin^2 2\theta]$ will reproduce that found for the usual case $f_s = 1$ modulo a “rigid” shift towards larger values of the mixing angle (see Sec. IV). The form of the contours will be altered in a different way when, as predicted by the DW mechanism, the relic abundance depends on the mass-mixing parameters (see Sec. V).

III. CONSTRAINTS FROM THE LYMAN- α FOREST

Massive neutrinos affect the cosmological evolution through two distinct effects. Firstly, in the early universe, they are relativistic and therefore contribute to the overall radiation budget of the universe, shifting the epoch of matter-radiation equality. Secondly, neutrinos erase fluctuations on scales smaller than the horizon size at the epoch when their kinematics becomes non-relativistic – the so-called free-streaming length [71]. For neutrinos under discussion here, the first effect is completely negligible while the second one can leave important imprints on structure formation which are detectable by Ly- α forest measurements. Indeed, these observations are directly sensitive to the free-streaming length which can be roughly expressed as [72]

$$\lambda_{\text{FS}} \simeq 1.2 \text{ Mpc} \left(\frac{\text{keV}}{m_s} \right) \frac{\langle p/T \rangle}{3.15}, \quad (8)$$

where $\langle p/T \rangle$ is the mean momentum over temperature for the sterile neutrino distribution. To impose constraints at such low length scales (\lesssim Mpc), one needs a probe of the small-scale matter power spectrum at high redshift, where the information on the primordial fluctuations has not yet been completely lost due to non-linear evolution. The Ly- α forest at redshifts 2-4 satisfies both requirements, constituting the most suitable probe of WDM [42]. Two recent and independent Ly- α analyses have provided very stringent lower bounds on the neutrino mass. Assuming that *all* the dark matter is made of sterile neutrinos and that they

are produced via non-resonant oscillations, a lower bound of 13 keV (at 95% C.L.) has been determined in [43], and a slightly weaker limit of 10 keV (at 95% C.L.) has been obtained in [44].

The most appropriate approach to constrain mixed models with $f_s < 1$ (we assume that the remaining fraction $(1 - f_s)$ of dark matter is made of CDM) would be by running a grid of hydrodynamical simulations in order to relate the observed Ly- α flux power spectrum with the expanded set of parameters considered here. This exceeds the scope of this work, and we instead adopt a different method which allows us to obtain reliable constraints simply rescaling the ones found in [43] for the case $f_s = 1$.

Assuming fiducial values for all cosmological parameters, we calculate the growth of perturbations including a mixed contribution of WDM (f_s) and of CDM ($1 - f_s$) in the code CAMB [73], incorporating the ν_s relic abundance through the relation

$$\Omega_s h^2 = \beta \left(\frac{m_s}{93.2 \text{eV}} \right), \quad (9)$$

where β is a suppression factor and we assume that sterile neutrinos possess a thermal momentum distribution. Recent calculations [74, 75] have shown that the real distribution exhibits appreciable deviations from the thermal form, which can be roughly approximated by a moderate shift of the average momentum toward lower values [74, 75]. This implies [see Eq. (8)] smaller free-streaming lengths and a consequent weakening of the lower bounds on the mass derived with the assumed approximation of a thermal distribution. The limit of 13 keV quoted in [43] already accounts for a 10% correction ($\langle p/T \rangle \sim 0.9$) as evaluated in [74]. Since the calculations [75] indicate deviations as large as $\simeq 20\%$ ($\langle p/T \rangle \sim 0.8$ for masses of 10 keV), we have conservatively rescaled the lower bound obtained in [43] by a further factor 0.9, thus adopting for the pure WDM case ($f_s = 1$) the reference lower bound $m_s \gtrsim 11.5$ keV.

Due to their pencil-beam nature, Ly- α measurements effectively probe the projected 1D flux power spectrum rather than the full 3D power spectrum. This implies that small-scale modes are projected onto much larger modes [43], with enhanced sensitivity on the scales of interest. Therefore, for each model (defined by the values of f_s and m_s), we integrate the resulting 3D linear power spectrum into the relevant 1D spectrum, using the relation

$$P_{1D}(k) = \frac{1}{2\pi} \int_k^\infty P_{3D}(k) k dk. \quad (10)$$

In order to derive lower limits on the neutrino mass from those already calculated in [43] for the case of pure WDM ($f_s = 1$), we adopt the following rescaling procedure [76]. For a model with a WDM fraction $f_s < 1$, we find the value of the neutrino mass that produces a suppression of the 1D power spectrum at the fiducial pivot wavenumber $k_f = 2h \text{ Mpc}^{-1}$ equal to that one obtained (for a larger value of the mass) in the case $f_s = 1$. Once the confidence level (C.L) at which a given mass is disfavored in the pure WDM case is provided, we assume that the values of the mass calculated as above for the models with $f_s < 1$ are disfavored at the same C.L.

Our procedure can be visualized in Fig. 2 which displays in the plane $[m_s, f_s]$ the iso-contours of the fractional suppression of the 1D matter power spectrum obtained for mixed (CDM + WDM) models with respect to the case of pure CDM. The values refer to the pivot scale $k = 2h \text{ Mpc}^{-1}$. The region under the thick solid line is excluded at the 2σ level and corresponds to a fractional suppression of $\sim 23\%$, which is the value found in [43] for

the case of pure WDM corresponding to the quoted 2σ lower bound on the neutrino mass. We observe that for small values of the relic abundance the lower limits depart from the power-law behavior displayed at large values, indicating a loss of sensitivity of the Ly- α measurements.

Although we have chosen the pivot wavenumber $k_f = 2h \text{ Mpc}^{-1}$ as this is the scale where SDSS Ly- α data are most sensitive [43], we have checked that our rescaling procedure returns stable results with respect to possible different choices of the pivot wavenumber in the range (1-5 $h \text{ Mpc}^{-1}$). In fact, a different choice of k_f in such range alters the lower limits by less than 10%, provided that sufficiently high values of the WDM fraction ($f_s \gtrsim 0.1$) are considered. For smaller values of f_s , the discrepancies become more pronounced and our procedure should be replaced by a more accurate treatment involving detailed simulations. We also observe that our rescaling procedure tacitly assumes that the change of cold to warm dark matter fraction affects just the linear power spectrum while leaving the transfer functions from the linear 1D power spectrum to the observed flux power spectrum unchanged. Corrections to this simple approximation could arise since the 1D power spectrum probes very high k modes which are probably significantly affected by the Jeans smoothing, non-linear coupling from larger scales and redshift-space distortions [77]. Therefore, dedicated hydrodynamical simulations are required in order to render our conclusions more quantitative.

IV. THEORETICAL PREDICTIONS AND EXPERIMENTAL CONSTRAINTS

In this section we will show how the constraints coming from X-ray and Ly- α data relate to the theoretical restrictions imposed by non-resonant production by confronting the usual case of dominant dark matter ($f_s = 1$) with a representative case in which it is subdominant ($f_s = 0.2$). The results of this sections will serve also as a guide for the interpretation of the more general results presented in the next section.

For our purposes we use the theoretical calculations performed in [75]. Although similar calculations have been recently performed [74], which are in substantial agreement with those presented in [75], the latter incorporate the most conservative evaluation of the hadronic uncertainties affecting the production process. Furthermore, fitting formulae valid in the whole range of mass and mixing parameters explored here are provided which allow us draw iso-abundance curves in the mass-mixing plane and to incorporate the theoretical predictions in the analysis. According to the calculations performed in [75], after a slight change in the notation, the relic abundance of sterile neutrinos can be conveniently expressed as

$$\Omega_s h^2 \simeq 0.275 \left(\frac{\sum_\alpha C_\alpha(m_s) \theta_\alpha^2}{\sum_\alpha \theta_\alpha^2} \right) \left(\frac{m_s}{\text{keV}} \right)^2 \left(\frac{\sin^2 2\theta}{10^{-7}} \right), \quad (11)$$

where the first term in parentheses embeds a mild dependence on the neutrino mass and on the flavor structure⁸ through the slowly varying functions C_α , which are directly evaluated in [75]. From direct comparison of Eqs. (9) and (11), we observe that the suppression factor β in Eq. (9) is related to the production mechanism. In particular, once the relic abundance and the mass are fixed, the factor β is unequivocally determined by the mixing angles. This dependence, together with the deviations from the thermal distribution, distinguishes the case of (out-of-equilibrium) production via non-resonant oscillations from the case of early

⁸ The functions C_α exhibit a moderate hierarchy [75] ($C_e > C_\mu > C_\tau$).

decoupling (in equilibrium), where an analogous suppression factor is instead related to the number of relativistic degrees of freedom at the time of decoupling [78].

The fitting formulae presented in [75] provide the relation that mass and mixing parameters must satisfy if sterile neutrinos constitute all the amount of dark matter. These are derived imposing $\Omega_s = \Omega_{\text{dm}}$ in Eq. (11), and thus correspond to the case $f_s = 1$. Given the form of Eq. (11), one can obtain fitting formulae for the fractional relic abundance simply rescaling those ones valid for the case $f_s = 1$. In particular, for the best estimate of the hadronic effects, one gets the average⁹ abundance [75]

$$\log_{10}(f_s^{\text{ave}}) = +0.17 + 1.84 \log_{10}\left(\frac{m_s}{\text{keV}}\right) + \log_{10}\left(\frac{\sin^2 2\theta}{10^{-7}}\right), \quad (12)$$

which we will use as the reference estimate in our analysis. Taking into account the hadronic uncertainties, the authors of [75] determine two extreme cases, corresponding respectively to the minimal

$$\log_{10}(f_s^{\text{min}}) = -0.07 + 1.74 \log_{10}\left(\frac{m_s}{\text{keV}}\right) + \log_{10}\left(\frac{\sin^2 2\theta}{10^{-7}}\right), \quad (13)$$

and to the maximal

$$\log_{10}(f_s^{\text{max}}) = +0.62 + 1.74 \log_{10}\left(\frac{m_s}{\text{keV}}\right) + \log_{10}\left(\frac{\sin^2 2\theta}{10^{-7}}\right), \quad (14)$$

abundances that can be produced for given mass-mixing parameters. These estimates constitute two extreme cases in that they have been obtained by “pushing” all the errors induced by different and in principle independent sources of uncertainty¹⁰ towards the same direction. Lacking a precise definition of their statistical significance, we will adopt the conservative choice to interpret them as 2σ limits in our analysis.

In order to show how the constraints imposed by X-ray and Ly- α data relate to the theoretical predictions, we superimpose in Fig. 3 all the (2σ) experimental restrictions obtained for the two fixed values $f_s = 1$ (left panel) and $f_s = 0.2$ (right panel) to the theoretical curves corresponding to these same values and obtained by Eqs. (12-14). In both panels, the region above the descending thick solid curve is excluded by the X-ray analysis while the region below the thick horizontal line is forbidden by Ly- α . The inclined dashed line corresponds to the best estimate given by Eq. (12), while the other two dotted lines represent the two extreme cases of Eqs. (13-14).

In the left panel, corresponding to the usual case $f_s = 1$ (see Refs. [37, 44] for analogous plots), the strong tension existing between experimental constraints and theoretical predictions is clearly evidenced: the theoretical curves lie in the region which is excluded by X-ray data, by Ly- α data or by both sets of data. In particular, looking at the intersections points between the theoretical curve and the border of the regions excluded by X-ray and Ly- α data one find the incompatible limits $m_s \lesssim 7$ keV and $m_s \gtrsim 11.5$ keV respectively. Hence, as expected, the dominant case $f_s = 1$ seems strongly disfavored.

⁹ Here, we have taken the average of the two cases respectively dubbed as “case 1, mean” and “case 2, mean” in [75], obtained for two extreme flavor structures.

¹⁰ These are mainly the uncertainties on the equation-of-state (EOS) and on the hadronic scattering processes [75].

In the right panel, all the curves (including the theoretical one) refer to fractional abundance $f_s = 0.2$. Here the iso-abundance lines move (for a fixed mass) toward noticeably smaller values of the mixing angle. On the contrary, as discussed in Sec. II, the X-ray limits become less stringent “moving” toward larger (by a factor $1/f_s = 5$) values of the mixing angle, while the Ly- α lower bound on the mass drastically decreases ($m_s \gtrsim 2.5$ keV) as discussed in Sec. III. The net result is that for subdominant dark matter with fractional abundance $f_s = 0.2$ a region for the mass-mixing parameters is permitted. If one adopts the best estimate for the relic abundance, this region corresponds to the segment of the dashed line delimited by the two regions excluded respectively by X-ray and Ly- α data. The end points of such segment correspond to values of the neutrino mass in the range (2.5-16 keV) and to values of the mixing angle in the range (9×10^{-11} – 2.5×10^{-9}). Intuitively one can expect that such ranges would change (reducing) for increasing values of the fractional abundance f_s until they disappear for sufficiently high values of f_s . This is the case as we will show by the quantitative analysis performed in the next section.

V. CONSTRAINTS ON THE DODELSON-WIDROW SCENARIO

In this section we will show how the results coming from X-ray and Ly- α data can be used to put constraints on the parameters which govern non-resonant production of sterile neutrinos in the early universe. In order to determine the mass-mixing parameters which are compatible with the experimental data, we impose that for each point of the mass-mixing plane, the relic abundance is the one determined by the theoretical calculations.

Figure 4 shows the results of such procedure for the three different estimates provided by Eqs. (12-14). The first panel corresponds to the “average” case [Eq. (12)], while the second and third panels represent respectively the two extreme cases of lowest [Eq. (13)] and highest [Eq. (14)] production efficiencies. In each of the three panels the solid curve delimits the parameter region (below) allowed at 2σ level, while the dotted lines represent iso-abundance contours. The left upper branch of the curve is determined by the X-ray constraints which now display a different behavior with respect to those presented in Fig. 3. Indeed, the relic abundance is not fixed *a priori* but varies with the parameters. Consequently, the limits on the neutrino mass now decrease faster with the mixing angle due to the corresponding increase of the relic abundance along the curve. As already observed in [49] these limits are less stringent than those obtained for the case $f_s = 1$ (see the left panel of Fig. 3), thus leaving room for a sterile neutrino explanation of the pulsar kicks. The allowed region is limited on the right by the fast descending branch determined by Ly- α measurements which, fixing a lower bound on the mass, indirectly limits also the mixing angle. The two branches converge for increasing values of f_s “closing” the allowed region in correspondence of a maximum value of the relic abundance (evidenced by a dashed segment) which depends on the assumed theoretical calculation. We observe that the left upper branch of the allowed region in the top panel of Fig. 4 is similar to that one determined in [49] using the same procedure. However, since only the X-ray data are considered in [49], the right lower branch of the allowed region is determined in [49] by the “overclosure” condition ($f_s = 1$), which is less restrictive than the constraints we obtain including also the Ly- α data. Moreover, we stress that only the inclusion of both set of data (X-ray and Ly- α) is able to jointly constrain the fractional abundance. The comparison of the three panels of Fig. 4 allows a qualitative evaluation of the impact of the theoretical uncertainties. In particular, the allowed region is subject to appreciable changes, enlarging (reducing) for lower (higher) production efficiencies

and the upper limit on the abundance is subject to noticeable fluctuations in the range (0.55-0.75).

In order to incorporate such uncertainties in a quantitative way in our analysis we allow the fractional abundance f_s to vary around its average value [determined by Eq. (12)] according to a log-normal¹¹ distribution with standard deviation taken equal to one half of the excursion (respect to the average) determined by the two extreme cases in Eqs. (13-14). This corresponds to adding a penalty factor¹² η to the total χ^2

$$\chi^2 = \chi_{\text{X-ray}}^2(\sin^2 2\theta, m_s, f_s) + \chi_{\text{Ly-}\alpha}^2(m_s, f_s) + \eta(\sin^2 2\theta, m_s, f_s), \quad (15)$$

defined as

$$\eta = \left[\frac{\log_{10}(f_s) - \log_{10}(f_s^{\text{ave}})}{\Delta \log_{10}(f_s)} \right]^2, \quad (16)$$

with 1σ (asymmetric) errors given by

$$\Delta \log_{10}(f_s) = 0.5 [\log_{10}(f_s^{\text{max}}) - \log_{10}(f_s^{\text{ave}})] \quad (f_s > f_s^{\text{ave}}), \quad (17)$$

$$\Delta \log_{10}(f_s) = 0.5 [\log_{10}(f_s^{\text{ave}}) - \log_{10}(f_s^{\text{min}})] \quad (f_s < f_s^{\text{ave}}). \quad (18)$$

Then, in order to obtain the allowed region for the mass-mixing parameters, we marginalize the χ^2 in Eq. (15) with respect to the parameter f_s . Figure 5 shows the allowed region (at the 2σ and 3σ levels) obtained following this procedure. As expected, the 2σ region is slightly enlarged respect to that one obtained for the ‘‘average’’ case (first panel of Fig. 4). Note that in this plot iso-abundance contours cannot be drawn since the value of f_s is now determined by the marginalization process and thus depends on the confidence level. In particular, the maximum value allowed at the 2σ level turns out to be $f_s \lesssim 0.7$ which is slightly more stringent than the absolute upper limit (0.75) obtained for the extreme case of the highest production efficiency (third panel of Fig. 4). In fact, any departure from the best estimated abundance is now hindered by the counterbalancing effect of the penalty factor η . Furthermore, we find that the case in which sterile neutrinos constitute all the amount of dark matter ($f_s = 1$) is disfavored at the $\sim 3\sigma$ level.

As already noted in the previous section (see the discussion concerning the case $f_s = 0.2$), for a given value of the relative abundance f_s produced via non-resonant oscillations, the experimental data determine two allowed ranges for the mass and the mixing angle respectively. From Fig. 4 one can see that the amplitude of such ranges gradually diminishes until it eventually becomes zero for the maximum value allowed for the abundance. This behavior can be effectively visualized marginalizing the χ^2 in Eq. (15) with respect to one of the mass-mixing parameters. The result of such an exercise is shown in Fig. 6 which shows the (2σ and 3σ) ranges for values of $f_s > 0.1$, where our Ly- α rescaling procedure furnishes robust results.¹³ In the first panel (where the mass is projected out), the lower bound on

¹¹ The log-normal distribution is more suited to treat the large hadronic uncertainties.

¹² Note that the three cases considered above (in which the relic abundance is univocally fixed by the mass and mixing parameters) are formally recovered introducing as penalty factor a Dirac delta function centered respectively on the average, lowest or highest abundance.

¹³ It has been recently shown [41] that gamma-ray line emission searches can improve current X-ray limits in the region of very large masses and small mixing angles, which is relevant for very low values of the relic abundance ($f_s < 0.1$).

the mixing angle is determined by X-ray observations, while the upper bound is fixed by Ly- α measurements. The situation is reversed in the second panel (here the mixing angle is projected out) where the range allowed for the neutrino mass is limited from below by Ly- α measurements, and the upper bound is provided by X-ray observations.

Although a direct measurement of the relic abundance of sterile neutrinos is not feasible, an indirect evidence for a mixed (WDM+CDM) scenario may constitute a realistic possibility. In this case, one might ask which parameters can give rise to sterile neutrinos in the right amount required to make the WDM component. Figure 6 provides an immediate and quantitative answer to this question showing at a glance where the DW model should “live”. As expected the allowed ranges gradually reduce for increasing values of f_s until they eventually shrink in correspondence of the maximum value allowed for the relic abundance.

We close this section with a final cautionary remark. As already stressed, the upper limit that we found on the relic abundance is valid only under the assumption that sterile neutrinos are produced *solely* through the simplest production mechanism involving non-resonant oscillations. It can be evaded considering exotic models such as resonant oscillations [47] boosted by large primeval lepton asymmetries, generation mechanisms operative during [48] or prior to [49] oscillations or low reheating temperatures [50, 51]. Therefore, further investigation of these possibilities is important to prevent a viable dark matter candidate from being dismissed prematurely. In this context our results could serve as a quantitative guide for exploring possible mechanisms which are expected to act in synergy with the production via non-resonant oscillations.

VI. CONCLUSIONS

In light of recent results which seem to disfavor keV sterile neutrinos as viable dark matter candidates, we have revisited the constraints attainable on the parameters which govern the Dodelson-Widrow (DW) production mechanism. Relaxing the usual hypothesis that sterile neutrinos must account for all the dark matter content ($\Omega_s = \Omega_{\text{dm}}$), we have shown how the X-ray and Ly- α measurements can be reinterpreted in the subdominant case ($\Omega_s < \Omega_{\text{dm}}$). In addition, we have shown how the current data provide us with a conservative upper bound on the fraction of sterile neutrinos produced via the DW mechanism, which is robust with respect to the large uncertainties affecting the theoretical estimates. More sensitive X-ray observations, more quantitative Ly- α analyses, and a reduction of the theoretical uncertainties, all will need to play a crucial role in order to improve our limits.

Acknowledgments

We are grateful to V. Antonuccio, E. Lisi, P. McDonald, D. Montanino, S. Sarkar, and U. Seljak for useful discussions. A. Palazzo is supported by INFN, A. Slosar by Oxford Astrophysics.

-
- [1] J.J. Dalcanton and C.J. Hogan, *Astrophys. J.* **561**, 35 (2001).
 - [2] F.C. van den Bosch and R.A. Swaters, *Mon. Not. Roy. Astron. Soc.* **325**, 1017 (2001).
 - [3] R.A. Swaters, B.F. Madore, F.C.V. Bosch and M. Balcells, *Astrophys. J.* **583**, 732 (2003).

- [4] G. Gentile, P. Salucci, U. Klein, D. Vergani and P. Kalberla, *Mon. Not. Roy. Astron. Soc.* **351**, 903 (2004).
- [5] J.D. Simon, A.D. Bolatto, A. Leroy, L. Blitz and E.L. Gates, *Astrophys. J.* **621**, 757 (2005).
- [6] E. Zackrisson, N. Bergvall, T. Marquart and G. Ostlin, *Astron. Astrophys.* **452**, 857, (2006).
- [7] R. Kuzio de Naray, S.S. McGaugh, W.J.G. de Blok and A. Bosma, *Astrophys. J. Suppl.* **165**, 461 (2006).
- [8] T. Goerdt, B. Moore, J.I. Read, J. Stadel and M. Zemp, *Mon. Not. Roy. Astron. Soc.* **368**, 1073 (2006).
- [9] L.E. Strigari, J.S. Bullock, M. Kaplinghat, A.V. Kravtsov, O.Y. Gnedin, K. Abazajian and A.A. Klypin, *Astrophys. J.* **652**, 306 (2006).
- [10] G. Kauffmann, S.D.M. White and B. Guiderdoni, *Mon. Not. Roy. Astron. Soc.* **264**, 201 (1993).
- [11] A.A. Klypin, A.V. Kravtsov, O. Valenzuela and F. Prada, *Astrophys. J.* **522**, 82 (1999).
- [12] B. Moore, S. Ghigna, F. Governato, G. Lake, T. Quinn, J. Stadel and P. Tozzi, *Astrophys. J.* **524**, L19 (1999).
- [13] B. Moore, T. Quinn, F. Governato, J. Stadel and G. Lake, *Mon. Not. Roy. Astron. Soc.* **310**, 1147 (1999).
- [14] A.R. Zentner and J.S. Bullock, *Astrophys. J.* **598**, 49 (2003).
- [15] P. Bode, J.P. Ostriker and N. Turok, *Astrophys. J.* **556**, 93 (2001).
- [16] V. Avila-Reese, P. Colin, O. Valenzuela, E. D'Onghia and C. Firmani, *Astrophys. J.* **559**, 516 (2001).
- [17] B. Brahmachari, S. Choubey and R.N. Mohapatra, *Phys. Lett. B* **536**, 94 (2002).
- [18] Z.G. Berezhiani and R.N. Mohapatra, *Phys. Rev. D* **52**, 6607 (1995).
- [19] E.J. Chun and H.B. Kim, *Phys. Rev. D* **60**, 095006 (1999).
- [20] P. Langacker, *Phys. Rev. D* **58**, 093017 (1998).
- [21] K.N. Abazajian, G.M. Fuller and M. Patel, *Phys. Rev. Lett.* **90**, 061301 (2003).
- [22] T. Asaka, S. Blanchet and M. Shaposhnikov, *Phys. Lett. B* **631**, 151 (2005).
- [23] S. Dodelson and L.M. Widrow, *Phys. Rev. Lett.* **72**, 17 (1994).
- [24] C. Athanassopoulos *et al.*, *Phys. Rev. Lett.* **77**, 3082 (1996); **81**, 1774 (1998); A. Aguilar *et al.* *Phys. Rev. D* **64**, 112007 (2001).
- [25] A.A. Aguilar-Arevalo *et al.* [The MiniBooNE Collaboration], arXiv:0704.1500 [hep-ex].
- [26] K. Abazajian, G.M. Fuller and W.H. Tucker, *Astrophys. J.* **562**, 593 (2001).
- [27] A.D. Dolgov and S.H. Hansen, *Astropart. Phys.* **16**, 339 (2002).
- [28] M. Drees and D. Wright, arXiv:hep-ph/0006274.
- [29] A. Boyarsky, A. Neronov, O. Ruchayskiy, M. Shaposhnikov and I. Tkachev, *Phys. Rev. Lett.* **97**, 261302 (2006).
- [30] P.B. Pal and L. Wolfenstein, *Phys. Rev. D* **25**, 766 (1982).
- [31] V.D. Barger, R.J.N. Phillips and S. Sarkar, *Phys. Lett. B* **352**, 365 (1995) [Erratum-ibid. B **356**, 617 (1995)].
- [32] A. Boyarsky, A. Neronov, O. Ruchayskiy and M. Shaposhnikov, *Mon. Not. Roy. Astron. Soc.* **370**, 213 (2006).
- [33] S. Riemer-Sorensen, S.H. Hansen and K. Pedersen, *Astrophys. J.* **644**, L33 (2006).
- [34] K.N. Abazajian, M. Markevitch, S.M. Koushiappas and R.C. Hickox, *Phys. Rev. D* **75**, 063511 (2007).
- [35] A. Boyarsky, J. Nevalainen and O. Ruchayskiy, arXiv:astro-ph/0610961.
- [36] A. Boyarsky, J.W. den Herder, A. Neronov and O. Ruchayskiy, arXiv:astro-ph/0612219.

- [37] C.R. Watson, J.F. Beacom, H. Yuksel and T.P. Walker, Phys. Rev. D **74**, 033009 (2006).
- [38] A. Boyarsky, A. Neronov, O. Ruchayskiy and M. Shaposhnikov, Phys. Rev. D **74**, 103506 (2006).
- [39] S. Riemer-Sorensen, K. Pedersen, S.H. Hansen and H. Dahle, arXiv:astro-ph/0610034.
- [40] A. Boyarsky, O. Ruchayskiy and M. Markevitch, arXiv:astro-ph/0611168.
- [41] H. Yuksel, J.F. Beacom and C.R. Watson, arXiv:0706.4084 [astro-ph].
- [42] V.K. Narayanan, D.N. Spergel, R. Dave and C.P. Ma, Astrophys. J. Lett. **543**, L103 (2000).
- [43] U. Seljak, A. Makarov, P. McDonald and H. Trac, Phys. Rev. Lett. **97**, 191303 (2006).
- [44] M. Viel, J. Lesgourgues, M.G. Haehnelt, S. Matarrese and A. Riotto, Phys. Rev. Lett. **97**, 071301 (2006).
- [45] P. McDonald *et al.*, Astrophys. J. Suppl. **163**, 80 (2006).
- [46] M. Miranda and A.V. Maccio, arXiv:0706.0896 [astro-ph].
- [47] X.D. Shi and G.M. Fuller, Phys. Rev. Lett. **82**, 2832 (1999).
- [48] M. Shaposhnikov and I. Tkachev, Phys. Lett. B **639**, 414 (2006).
- [49] A. Kusenko, Phys. Rev. Lett. **97**, 241301 (2006).
- [50] G. Gelmini, S. Palomares-Ruiz and S. Pascoli, Phys. Rev. Lett. **93**, 081302 (2004).
- [51] C. E. Yaguna, JHEP **0706**, 002 (2007).
- [52] A. Kusenko and G. Segre, Phys. Lett. B **396**, 197 (1997).
- [53] A. Kusenko and G. Segre, Phys. Rev. D **59**, 061302(R) (1999).
- [54] G.M. Fuller, A. Kusenko, I. Mocioiu and S. Pascoli, Phys. Rev. D **68**, 103002 (2003).
- [55] A. Kusenko, Int. J. Mod. Phys. D **13**, 2065 (2004).
- [56] M. Barkovich, J.C.D'Olivo and R. Montemayor, Phys. Rev. D **70**, 043005 (2004).
- [57] J. Hidaka and G.M. Fuller, Phys. Rev. D **74**, 125015 (2006).
- [58] J. Hidaka and G.M. Fuller, arXiv:0706.3886 [astro-ph].
- [59] R. Barkana, Z. Haiman and J.P. Ostriker, Astrophys. J. **558**, 482 (2001).
- [60] N. Yoshida, A. Sokasian, L. Hernquist and V. Springel, Astrophys. J. **591**, L1 (2003).
- [61] M. Mapelli and A. Ferrara, Mon. Not. Roy. Astron. Soc. **364**, 2 (2005).
- [62] P.L. Biermann and A. Kusenko, Phys. Rev. Lett. **96**, 091301 (2006).
- [63] M. Mapelli, A. Ferrara and E. Pierpaoli, Mon. Not. Roy. Astron. Soc. **369**, 1719 (2006).
- [64] J. Stasielak, P.L. Biermann and A. Kusenko, Astrophys. J. **654**, 290 (2007).
- [65] E. Ripamonti, M. Mapelli and A. Ferrara, Mon. Not. Roy. Astron. Soc. **375**, 1399 (2007).
- [66] D.N. Spergel *et al.* [WMAP Collaboration], Astrophys. J. Suppl. **170**, 377 (2007).
- [67] F. Marshall *et al.*, Astrophys. J. **235**, 4 (1980).
- [68] D.E. Gruber, J.L. Matteson, L.E. Peterson and G.V. Jung, Astrophys. J. **520**, 124 (1999).
- [69] E. Masso and R. Toldra, Phys. Rev. D **60**, 083503 (1999).
- [70] G. Battaglia *et al.*, Mon. Not. Roy. Astron. Soc. **364**, 433 (2005) [Erratum-ibid. **370**, 1055 (2006)].
- [71] J.R. Bond, G. Efstathiou and J. Silk, Phys. Rev. Lett. **45**, 1980 (1980).
- [72] K. Abazajian, G.M. Fuller and M. Patel, Phys. Rev. D **64**, 023501 (2001).
- [73] A. Lewis *et al.*, Astrophys. J. Lett. **538**, 473 (2000).
- [74] K. Abazajian, Phys. Rev. D **73**, 063506 (2006).
- [75] T. Asaka, M. Laine and M. Shaposhnikov, JHEP **0606**, 053 (2006).
- [76] U. Seljak, private communication.
- [77] P. McDonald, private communication.
- [78] S. Colombi, S. Dodelson and L.M. Widrow, Astrophys. J. **458**, 1 (1996).

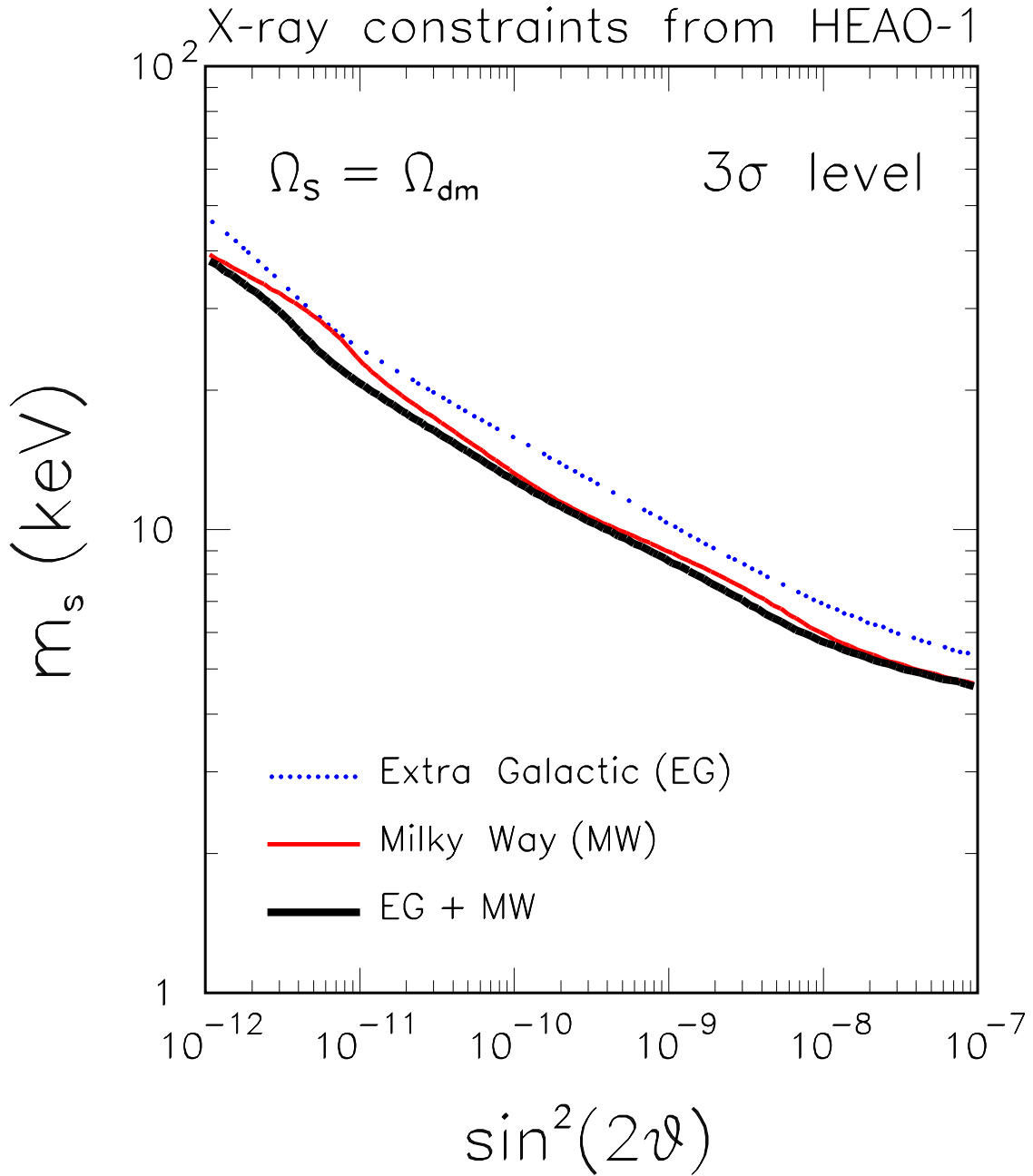


FIG. 1: Constraints (at the 3σ level) on mass and mixing parameters obtained from the spectral analysis of the HEAO-1 data under the assumption that sterile neutrinos account for all the dark matter content ($\Omega_s = \Omega_{\text{dm}}$). The bounds obtained including only the Milky Way (MW) contribution, only the extra-galactic (EG) contribution, and their sum are shown separately.

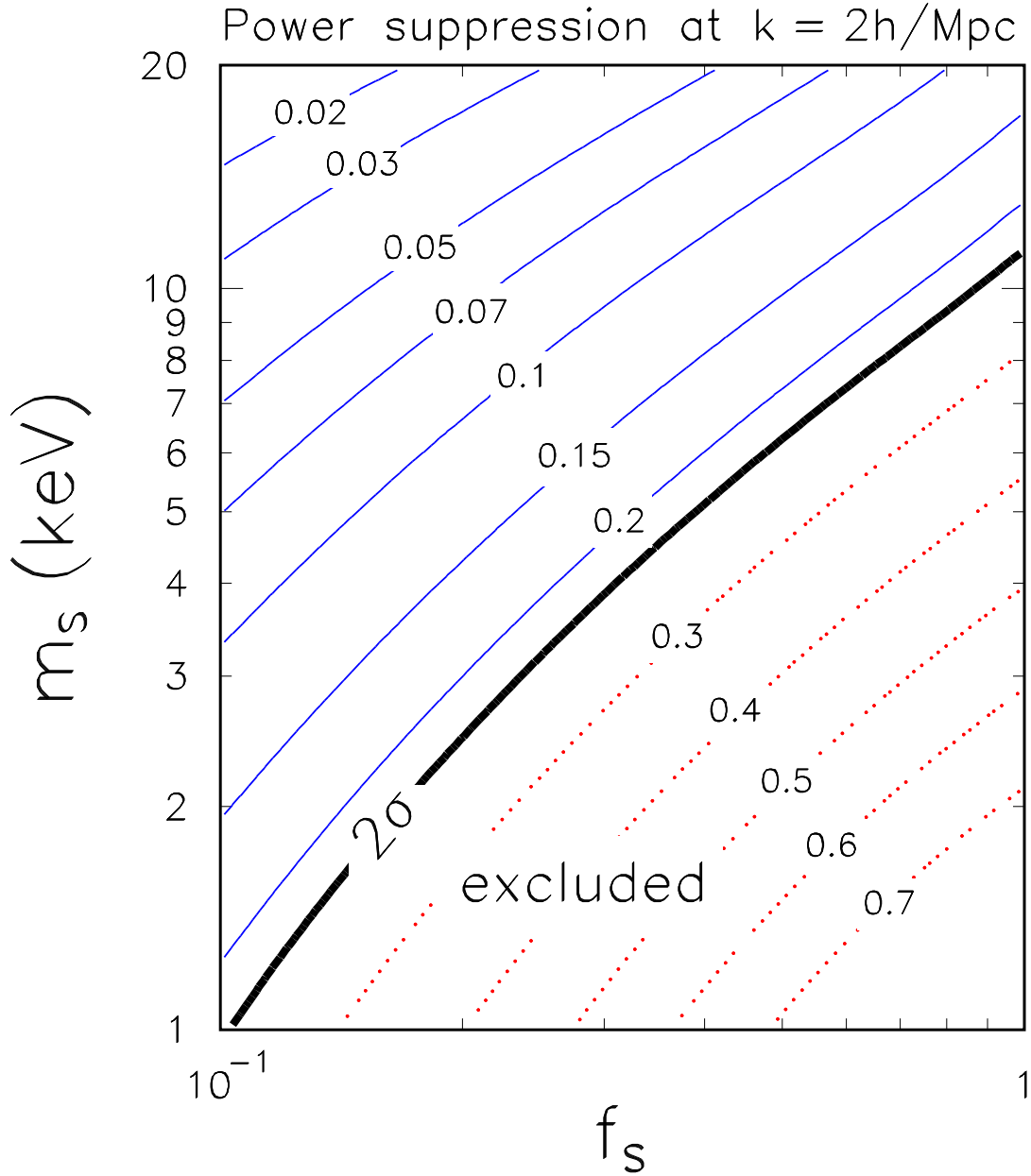


FIG. 2: Fractional suppression of the one dimensional matter power spectrum for mixed (CDM +WDM) models with respect to the case of pure CDM. The values refer to the pivot scale $k = 2h \text{ Mpc}^{-1}$. The region under the thick solid line is excluded at 2σ level by Lyman- α measurements. See the text for details.

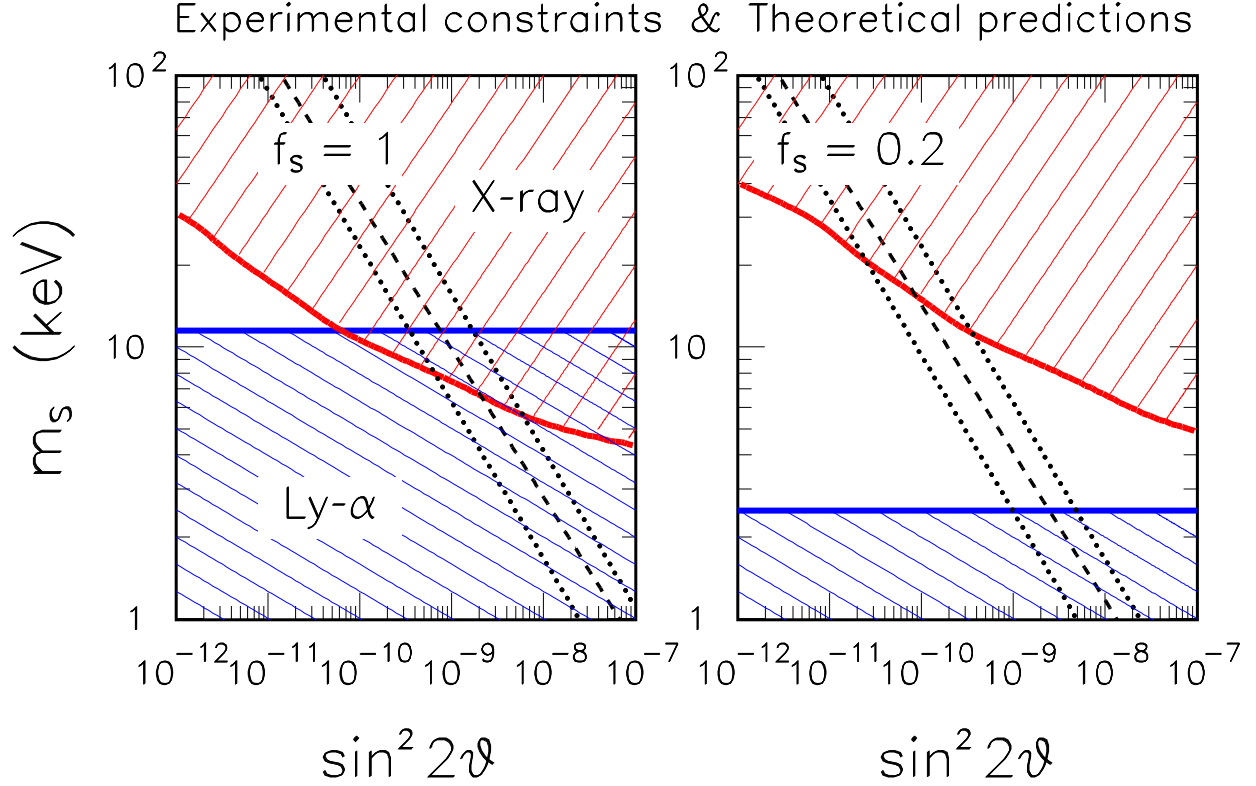


FIG. 3: Comparison of the constraints on mass-mixing parameters imposed by experimental data (X-ray and Ly- α) with the theoretical predictions obtained in [75] for the Dodelson-Widrow mechanism. The two panels confront the “usual” case $f_s = 1$ (left panel) with a representative case in which sterile neutrinos constitute only a fraction $f_s = 0.2$ of dark matter (right panel).

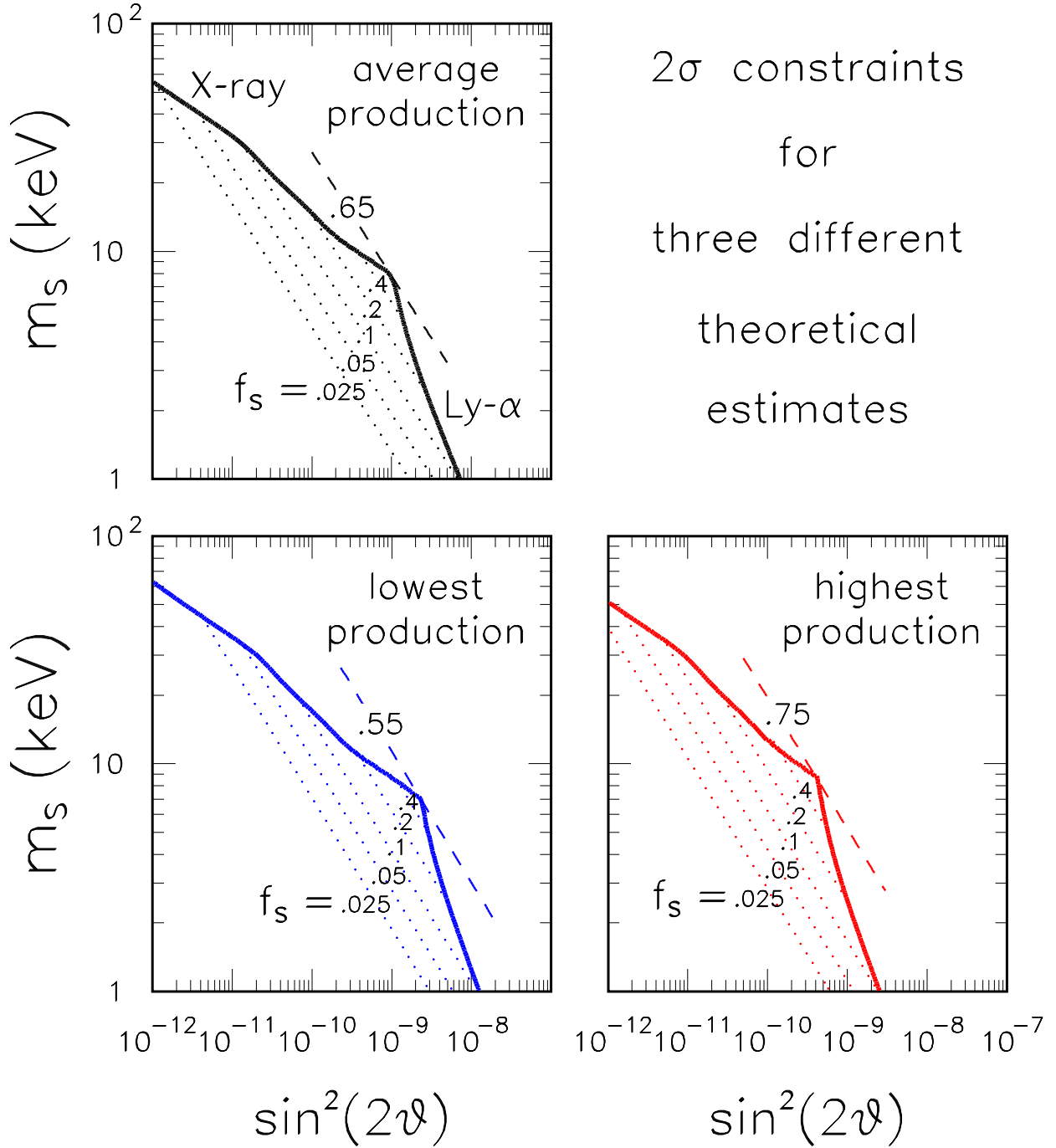


FIG. 4: Joint constraints from X-ray and Ly- α data on the mass-mixing parameters obtained for three different theoretical estimates of the relic abundance of sterile neutrinos produced via the Dodelson-Widrow mechanism. In each panel the allowed region lies under the solid curve, the dotted lines represent curves of constant sterile neutrino fractional abundance, while the dashed segment indicates its maximum value allowed in each case. In the first panel the “average” theoretical calculation obtained in [75] is used. In the last two panels the theoretical abundance is taken equal to the two extreme estimates determined in [75].

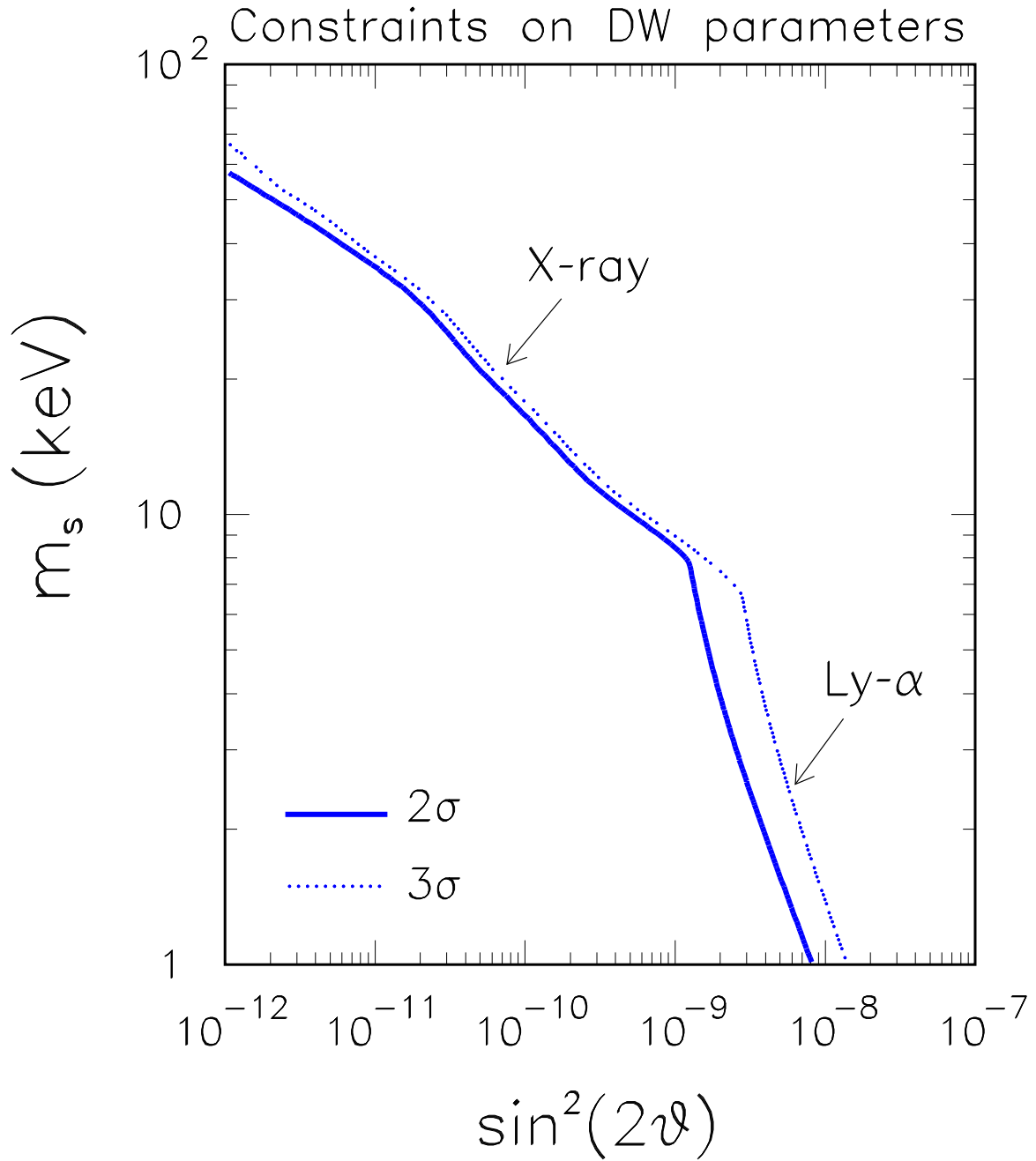


FIG. 5: Constraints on mass and mixing parameters governing the Dodelson-Widrow mechanism obtained by the joint analysis of X-ray and Ly- α data with the inclusion of the theoretical uncertainties. See the text for details.

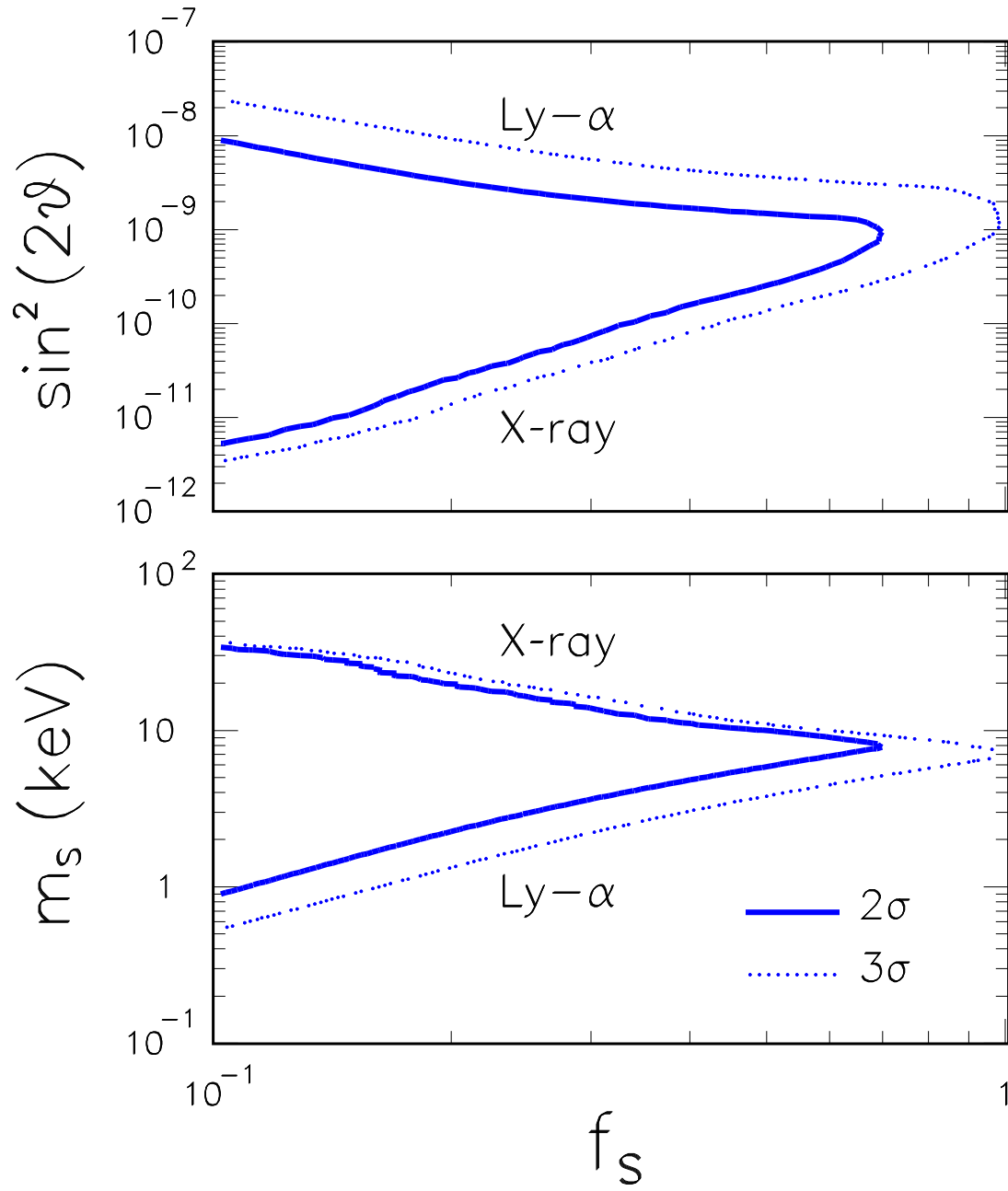


FIG. 6: Ranges allowed for the mixing angle (upper panel) and the neutrino mass (lower panel) as a function of the relic abundance obtained under the assumption of production via the Dodelson-Widrow mechanism.